A unifying model for elongational flow of polymer melts and solutions based on the interchain tube pressure concept

Manfred Hermann Wagner and Víctor Hugo Rolón-Garrido

Citation: AIP Conference Proceedings **1662**, 020001 (2015); doi: 10.1063/1.4918871
View online: http://dx.doi.org/10.1063/1.4918871
View Table of Contents: http://scitation.aip.org/content/aip/proceeding/aipcp/1662?ver=pdfcov
Published by the AIP Publishing

A Unifying Model for Elongational Flow of Polymer Melts and Solutions Based on the Interchain Tube Pressure Concept

Manfred Hermann Wagner[1, a)] and Víctor Hugo Rolón-Garrido[1, b)]

[1]*Chair of Polymer Engineering and Physics, Berlin Institute of Technology (TU Berlin), Fasanenstr. 90, D-10623 Berlin, Germany*

[a)]Corresponding author: manfred.wagner@tu-berlin.de
[b)]victor.h.rolongarrido@tu-berlin.de

Abstract. An extended interchain tube pressure model for polymer melts and concentrated solutions is presented, based on the idea that the pressures exerted by a polymer chain on the walls of an anisotropic confinement are anisotropic (M. Doi and S. F. Edwards, *The Theory of Polymer Dynamics*, Oxford University Press, New York, 1986). In a tube model with variable tube diameter, chain stretch and tube diameter reduction are related, and at deformation rates larger than the inverse Rouse time τ_R, the chain is stretched and its confining tube becomes increasingly anisotropic. Tube diameter reduction leads to an interchain pressure in the lateral direction of the tube, which is proportional to the 3rd power of stretch (G. Marrucci and G. Ianniruberto. Macromolecules **37**, 3934-3942, 2004). In the extended interchain tube pressure (EIP) model, it is assumed that chain stretch is balanced by interchain tube pressure in the lateral direction, and by a spring force in the longitudinal direction of the tube, which is linear in stretch. The scaling relations established for the relaxation modulus of concentrated solutions of polystyrene in oligomeric styrene (M. H. Wagner, Rheol. Acta **53**, 765-777, 2014, M. H. Wagner, J. Non-Newtonian Fluid Mech. http://dx.doi.org/10.1016/j.jnnfm.2014.09.017, 2014) are applied to the solutions of polystyrene (PS) in diethyl phthalate (DEP) investigated by Bhattacharjee et al. (P. K. Bhattacharjee et al., Macromolecules **35**, 10131-10148, 2002) and Acharya et al. (M. V. Acharya et al. AIP Conference Proceedings **1027**, 391-393, 2008). The scaling relies on the difference ΔT_g between the glass-transition temperatures of the melt and the glass-transition temperatures of the solutions. ΔT_g can be inferred from the reported zero-shear viscosities, and the BSW spectra of the solutions are obtained from the BSW spectrum of the reference melt with good accuracy. Predictions of the EIP model are compared to the steady-state elongational viscosity data of PS/DEP solutions. Except for a possible influence of solvent quality, linear and nonlinear viscoelasticity of entangled polystyrene solutions can thus be obtained from the linear-viscoelastic characteristics of a reference polymer melt and the shift of the glass transition temperature between melt and solution.

INTRODUCTION

The filament stretching technique has revealed very interesting and unexpected aspects of the steady-state elongational properties of polymer solutions and melts of monodisperse and polydisperse polymers [1-5], which are outside the predicting capabilities of the classical Doi-Edwards (DE) tube model. In elongational flow, the tube model with the so-called independent alignment assumption predicts an upper limit of the tensile stress equal to 5 times the plateau modulus, G_N [6]. This limiting stress is a consequence of the assumption of instantaneous chain retraction and therefore the absence of any chain stretching. In the DE model, the tube diameter is assumed to be constant, and the macroscopic stress is a consequence of chain orientation only, resulting in a scaling of the steady-state elongational viscosity at strain rates $\dot{\varepsilon}$ larger than the inverse reptation time according to $\dot{\varepsilon}^{-1}$. Relaxing the assumption of instantaneous chain retraction, various reptation-based models have invoked chain stretch when the deformation rate is larger than the inverse Rouse time τ_R of the chain [7-11], and these models seem to capture the essential features seen in the elongational viscosity of polymer solutions [1, 2, 12, 13], i.e. a decrease of the

Novel Trends in Rheology VI
AIP Conf. Proc. 1662, 020001-1–020001-20; doi: 10.1063/1.4918871

elongational viscosity proportional to $\dot{\varepsilon}^{-1}$ for elongation rates less than the inverse Rouse time, and a sudden increase at larger elongation rates.

In spectacular contrast to polymer solutions, elongational viscosity measurements of Bach et al. [4] on narrow molar mass distribution polystyrene melts revealed that the elongational viscosity scales approximately with $(\dot{\varepsilon}\tau_R)^{-1/2}$ in the nonlinear viscoelastic regime. To account for this behavior and relaxing the assumption of a constant tube diameter, Marrucci and Ianniruberto [14, 15] introduced an interchain pressure term arising from lateral forces between polymer chain and tube wall into the DE model, leading to a nonlinear stretch evolution equation and a specific tube diameter relaxation time τ_a, which limits chain stretching. However, their analysis was restricted to scalar arguments and to the steady-state viscosity. A full constitutive equation, which describes time-dependent as well as steady-state rheology of nearly monodisperse polymer melts was presented by Wagner et al. [16], and predictions are in excellent agreement with the elongational viscosity data of Bach et al. [4], Hassager [17], Nielsen et al. [5], and Rolón-Garrido et al. [18].

The tube diameter relaxation time introduced by Marrucci and Ianniruberto [14, 15] was expected to be proportional to the Rouse relaxation time, but the exact value of the proportionality constant remained elusive. By considering the limit of small chain stretch, Wagner and Rolón-Garrido [19, 20] showed that in the melt, the tube diameter relaxation time is equal to 3 times the Rouse stretch relaxation time of the chain, and proposed a combination of Rouse relaxation and tube diameter relaxation in agreement with experimental evidence of elongational flow data of monodisperse linear polymer melts. Wagner [21] extended this concept to bidisperse polymer systems consisting of a short and a long chain component, and demonstrated that the tube diameter relaxation time of the long chain component is increased in accordance with the expansion of the tube diameter due to dynamic tube dilation. Implementation of the dilation effect into the evolution equation of the stretch led to a quantitative description of the elongational behaviour of bidisperse polystyrene melts.

To clarify the difference in the elongational behavior of polymer melts and solutions, Huang et al. [22, 23] investigated elongational viscosities of two polystyrene melts as well as of several concentrated solutions with polymer volume fractions $\varphi \geq 44\%$ of the same polystyrenes in oligomeric styrene. Although the solutions did not show a significant decrease of the steady-state elongational viscosity proportional to $\dot{\varepsilon}^{-1}$ for elongation rates less than the inverse Rouse time and a sudden increase at larger elongation rates, these data may serve as a bridge towards the understanding of more dilute but still entangled solutions. Interestingly, Huang et al. [22, 23] were able to demonstrate that for polymer melts and solutions, storage and loss modulus as well as frequency and time can be shifted such that the linear-viscoelastic properties are identical provided that the number of entanglements is identical. However, the non-linear properties in strong extensional flow are remarkably different, and they reported that polymer solutions show much stronger extensional hardening than the corresponding melts. They speculated on a nematic interaction between the polymer and the oligomeric styrene [23]. The transient uniaxial viscosity data were also analyzed by Rasmussen and Huang [22, 23] using a modified version of the MSF model for nearly monodisperse linear polymers with finite extensibility. The authors concluded that the complex flow behaviour should be understood as resulting from a blend, with different dynamics in the polymer and solution phases.

A different approach to model the data set of Huang et al. [22, 23] was recently accomplished [24, 25]. Scaling relations for linear viscoelasticity and elongational viscosity of PS melts and concentrated PS solutions were presented based on the fact that the glass transition temperature of the bulk polymer is reduced in solution state. The experimental data in elongational flow of two monodisperse polystyrene melts and their solutions in three different oligomeric styrenes were found to be consistent with the assumption that the tube, i.e. the confinement of a test chain, is characterized by the orientation in the direction along the tube, and the diameter of the tube in the lateral dimension. Chain stretch is associated with a reduction of the tube diameter, and is balanced by a linear spring force in the longitudinal direction, which is characterized by the Rouse stretch relaxation time of the solution, and a nonlinear interchain tube pressure in the lateral direction, which at the reference temperature of 130°C, was shown to be governed by the Rouse time of the bulk polymer.

The objective of the present study is to extend the approach proposed by Wagner [24, 25] to the set of elongational viscosity data reported by Bhattacharjee et al. [1] and Acharya et al. [12] on two high molar mass polystyrenes dissolved in DEP.

EXPERIMENTAL DATA

The experimental data discussed correspond to those presented by Bhattacharjee et al. [1] and Acharya et al. [12], and are taken from Desai and Larson [11]. The polymers used were nearly monodisperse polystyrenes (PS) with molar masses of 3900 kg.mol^{-1} and 1950 kg.mol^{-1}, denoted as PS-3900 and PS-1950, respectively. PS-3900 was dissolved in DEP at concentrations of 10 wt.%, 15 wt.% and 17 wt.%, and PS-1950 at 20 wt.%, 15 wt.% and 10 wt.% concentrations. In the notation PS-*x*/DEP-*y*, *x* identifies the molar mass of the PS samples, while *y* indicates the solution concentration. DEP can be considered as a good solvent for PS at room temperature [26]. All experiments were conducted at constant strain rate using a filament stretching rheometer at ambient condition, i.e. 21.5°C [12]. The reference sample used in the analysis presented here is a nearly monodisperse PS melt of molar mass 545 kg.mol^{-1}, which was characterized at 130°C by Huang et al. [22]. Tables 1 and 2 display the material parameters of the reference polymer melt and the polymer solutions.

TABLE 1. Material parameters of reference melt PS-545k at 130°C, and solutions of PS-1950 of 20 wt.%, 15 wt.% and 10 wt.% in DEP at 21.5°C.

	PS-545k	**PS-1950/DEP-20**	**PS-1950/DEP-15**	**PS-1950/DEP-10**
φ (wt.%)	1	0.20	0.15	0.10
η_0 (Pa·s)	2.823×10^{9}	1.645×10^{4}	4.391×10^{3}	$3.68\text{x}10^{2}$
$a_T a_{Tg}$	1	$2.24\text{x}10^{-5}$	$1.59\text{x}10^{-5}$	$5.29\text{x}10^{-6}$
ΔT_g (K)	0	195.9	201.8	224.4
G_N (Pa)	2.57×10^{5}	8.35×10^{3}	4.69×10^{3}	2.09×10^{3}
τ_t (s)	58750	10.5	5.00	0.94
τ_c (s)	0.419	$2.34\text{x}10^{-4}$	$2.96\text{x}10^{-4}$	$2.22\text{x}10^{-4}$
τ_R (s) eq. (15)	776.8	0.22	0.16	0.053
τ_{Rexp} (s)	776.8	0.08	0.07	0.06

TABLE 2. Material parameters of reference melt PS-545k at 130°C, and solutions of PS-3900 of 17 wt.%, 15 wt.% and 10 wt.% in DEP at 21.5°C.

	PS-545k	**PS-3900/DEP-17**	**PS-3900/DEP-15**	**PS-3900/DEP-10**
φ (wt.%)	1	0.17	0.15	0.10
η_0 (Pa·s)	2.823×10^{9}	1.185×10^{5}	4.532×10^{4}	4.415×10^{3}
$a_T a_{Tg}$	1	$2.66\text{x}10^{-5}$	$1.55\text{x}10^{-5}$	$6.01\text{x}10^{-6}$
ΔT_g(K)	0	193.0	202.3	221.4
G_N (Pa)	2.57×10^{5}	6.03×10^{3}	4.69×10^{3}	2.09×10^{3}
τ_t (s)	58750	105	51.6	11.3
τ_c (s)	0.419	$3.85\text{x}10^{-4}$	$2.89\text{x}10^{-4}$	$2.52\text{x}10^{-4}$
τ_R (s) eq. (15)	776.8	1.06	0.62	0.24
τ_{Rexp} (s)	776.8	0.33	0.20	0.13

SCALING RELATIONS OF POLYSTYRENE MELTS AND SOLUTIONS

The glass transition temperatures of the solvents is much lower than the glass transition temperature T_{gm} of polystyrene melts, which for PS-545k is 107.5°C [22]. Therefore the glass transition temperature of the solutions, T_{gs}, is shifted by a temperature difference $\Delta T_g = T_{gm} - T_{gs}$ relative to the glass transition temperature T_{gm} of the melt to lower values. Considering the same reference temperature T_0=130°C, melt and solutions show different time-temperature shifting (Fig.1a). However, when analysing the shift factors a_T of PS-545k and PS-285k dissolved in oligomeric styrene (OS) as reported by Huang et al. [22], Wagner [24] found that by taking the shift of the glass transition temperature ΔT_g into account (Fig.1b), the shift factors of melts (ΔT_g=0) and solutions can consistently be described as

$$\log_{10}(a_T) = \frac{-c_1^0 (T + \Delta T_g - T_0)}{c_2^0 + (T + \Delta T_g - T_0)} - \log_{10}(a_{Tg}) \tag{1}$$

The WLF parameters at the reference temperature of T=130°C are $c_1^0 = 8.99$ and $c_2^0 = 81.53K$. The vertical shift factor a_{Tg} is given by

$$\log_{10}(a_{Tg}) = \frac{-c_1^0 \Delta T_g}{c_2^0 + \Delta T_g} \tag{2}$$

The validity of Eq. 1 for PS dissolved in OS is shown in Fig. 2. Excellent agreement was obtained between the temperature dependence of melt and solutions with polymer volume fractions φ between 44 und 72% in 1k, 2k and 4k OS, resulting in shifts of the glass transition temperature ΔT_g between 8 and 49K. Assuming a linear variation of T_g between the glass transition temperature of the melt and the glass transition temperature of the solvent, ΔT_g of all five solutions can be modelled by

$$\Delta T_g = \frac{63{,}000\text{K}\,\frac{\text{mol}}{\text{g}}}{M_{OS} - 350\,\frac{\text{mol}}{\text{g}}}(1-\phi) \tag{3}$$

Neglecting the constant in the denominator, this is similar to the Fox-Flory equation [27], i.e. ΔT_g is roughly inverse proportional to the molar mass M_{OS} of the oligomeric styrenes.

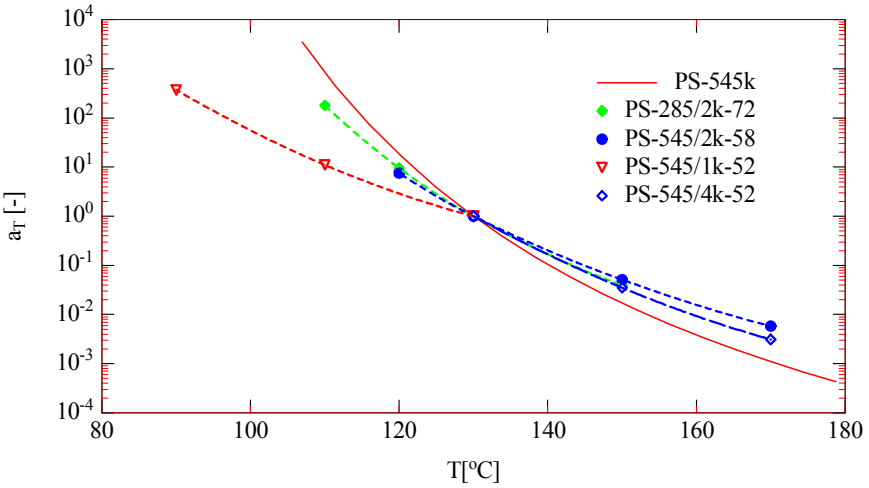

FIGURE 1a). Temperature shift factors a_T for polystyrene melt PS-545k and solutions at reference temperature of T_0=130°C as reported by Huang et al. [23]. Solid line for melt PS-545k is given by Eq. 1.

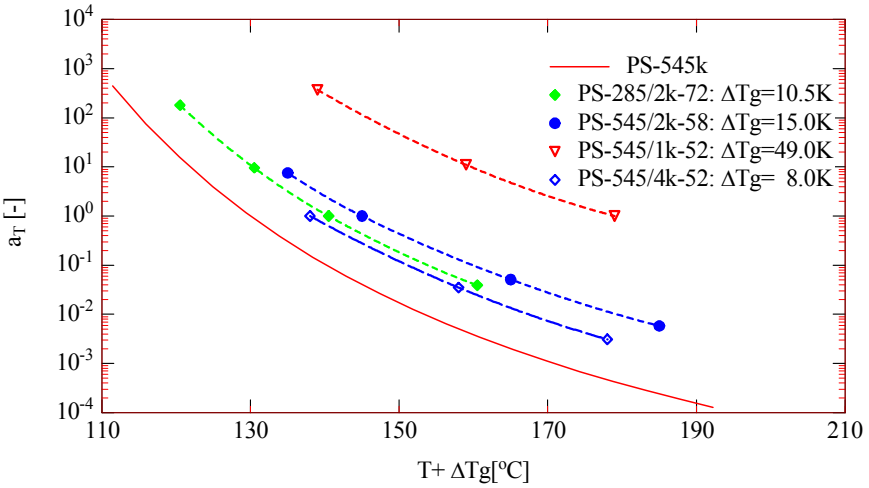

FIGURE 1b). Temperature shift factors a_T for polystyrene melt PS-545k and solutions at reference temperature of T_0=130°C as reported by Huang et al. [23]. Solid line for melt PS-545k is given by Eq. 1. Data horizontally shifted by $\Delta T_g = T_{gm} - T_{gs}$.

Also included in Fig. 2 are data for PS-545k dissolved in DBP with polymer fractions of 52 and 63% [22]. DBP is considered to be a good solvent for PS near room temperature [26]. Here, ΔT_g is much larger with ΔT_g=125 and 107K. The shift of the glass transition temperature ΔT_g as a function of the polymer fraction is shown in Fig. 3, and ΔT_g clearly depends on polymer concentration and the glass transition temperature T_g of the solvent.

For PS-3900 and PS-1950 dissolved in DEP, no temperature dependence of the linear-viscoelastic properties is available from literature. However, the shift factors can be inferred from the zero-shear viscosities reported by Arachya et al. [12] in the following way. The scaling of the zero-shear viscosity η_0 of a solution of PS with molar mass M_s dissolved in OS at T_0=130°C is given by [24]

$$\eta_0(T_0) = \eta_{0M}(T_0) a_M a_{Tg} \phi^{3.4} \tag{4}$$

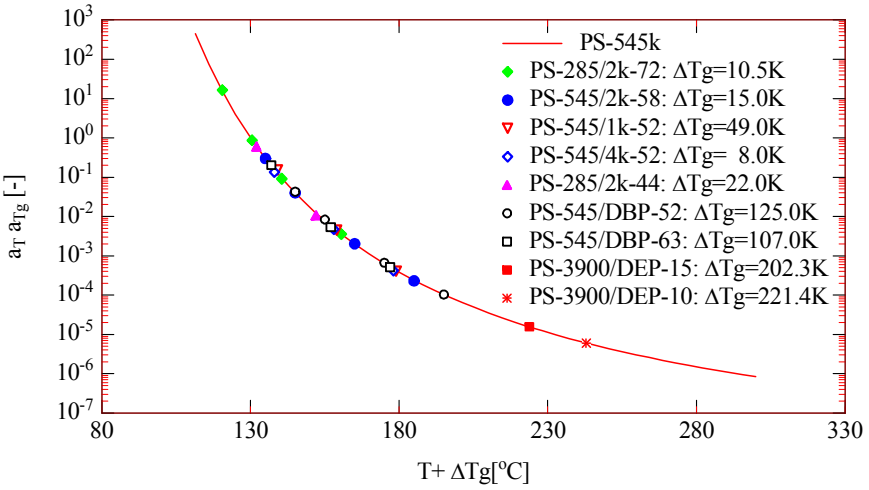

FIGURE 2. Temperature shift factors a_T for polystyrene melt and solutions for reference temperature of T_0=130°C as reported by Huang et al. [23] horizontally shifted by $\Delta T_g = T_{gm} - T_{gs}$ and vertically shifted by multiplication with shift factor a_{Tg}. Solid line is given by Eq. 1.

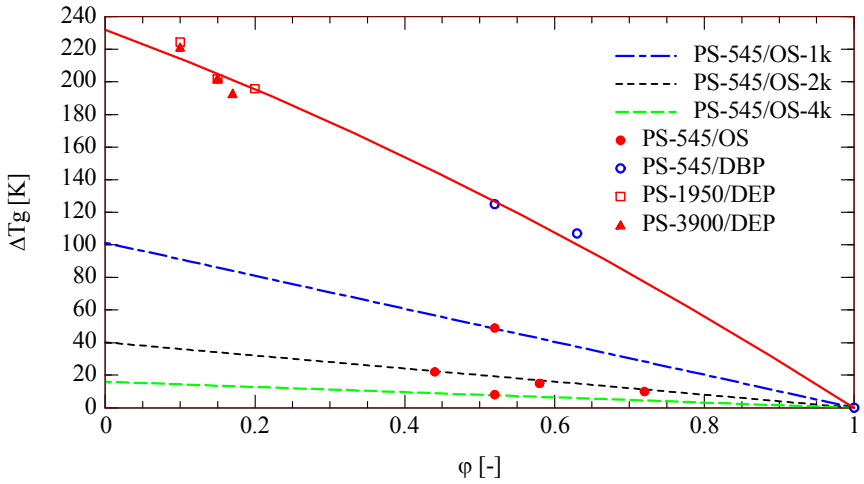

FIGURE 3. Shift of glass transition temperature ΔT_g as a function of polymer volume fraction. Dotted lines are given by Eq. 3, solid line by Eq. 10.

The index M denotes the reference PS melt (M = 545 kg.mol^{-1}), and a_M represents the molar mass shift factor,

$$a_M = \left(\frac{M_s}{M}\right)^{3.4} \tag{5}$$

M_s is 1950 kg.mol^{-1} and 3900 kg.mol^{-1}, respectively, in this study.

Assuming that Eq. 4 is valid also for the good solvent DEP in the same way as it was shown above to be valid for DBP in Fig. 2, and taking into account the temperature shift from the reference temperature T_0=130°C to the measuring temperature T_e=21.5°C by the shift factor a_T from Eq. 1 for $T = T_e$, the viscosity η_0 of the solution at temperature T_e is given by

$$\eta_0(T_e) = \eta_{0M}(T_0) a_M a_T a_{Tg} a_G \phi^{3.4} \tag{6}$$

The density shift factor a_G accounts for the change of entanglement density between T_e and T_0,

$$a_G = \frac{\rho(273\,°C + T_e)}{\rho_M(273\,°C + T_0)} \tag{7}$$

ρ is the density of the solution at the measuring temperature T_e, and ρ_M the density of the melt at temperature T_0. We take ρ = 1.111 g.cm^{-3} for DEP solutions, and ρ_M = 1 g.cm^{-3} for the melt.

The time-temperature shift factors $a_T a_{Tg}$ for the DEP solutions can then be obtained from Eq. 6 by using the experimentally determined zero-shear viscosities η_0 of the DEP solutions as reported by Arachya et al. [12], and η_{0M} of the reference melt from Huang et al. [22],

$$a_T a_{Tg} = \frac{\eta_0}{\eta_{0M} a_M a_G \phi^{3.4}} \tag{8}$$

When $a_T a_{Tg}$ is known, the shift ΔT_g in the glass-transition temperature of the solutions can be calculated from Eq. 1 as

$$\Delta T_g = T_0 - T_e - c_2^0 \frac{\log_{10}(a_T a_{Tg})}{\log_{10}(a_T a_{Tg}) + c_1^0} \tag{9}$$

$a_T a_{Tg}$ and ΔT_g of the DEP solutions are reported in Tables 1 and 2, and are included in Fig. 2 (for PS-3900/DEP-15 and PS-3900/DEP-10) and Fig. 3 (for all PS-3900/DEP solutions considered). The solid line in Fig. 3 is given by the following fit function for PS/DEP and PS/DBP,

$$\Delta T_g = 232 - 170\phi - 62\phi^2 \tag{10}$$

The dependence of ΔT_g on the polymer concentration is in qualitative agreement with the findings of Savin et al. [26], who found a smaller slope of $T_g(\varphi)$ in DSC measurements at low polymer concentrations for the system PS/DBP, and a higher slope for concentrated solutions.

Corresponding scaling relations were reported for the terminal and glassy relaxation times, τ_t and τ_c, respectively, for the system PS/OS [24], and are now generalized to

$$\tau_t(T_e) = \tau_{tM}(T_0) a_M a_T a_{Tg} \phi^{1.4} \tag{11}$$

and

$$\tau_c(T_e) = \tau_{cM}(T_0) a_T a_{Tg} \phi^{-2} \tag{12}$$

τ_{tM} and τ_{cM} are the terminal and glassy relaxation times of the reference PS melt at T_0, and are taken from Huang et al. [22]. For T_e=T_0, i.e. a_T = 1, the expressions of Wagner [24, 25] are naturally recovered. A dilution exponent of α = 1 was found to optimally describe the dependence of the plateau modulus G_N of PS diluted with PS oligomers [22, 23], and the same value of α was found from the experimental data of the plateau moduli of the system PS/DEP investigated by Bhattacharjee et al. [1], resulting in a scaling relation of the form

$$G_N = G_{NM} a_G \phi^2 \tag{13}$$

G_{NM} is the plateau modulus of the reference melt.

Another relevant quantity to describe molecular dynamics is the Rouse stretch relaxation time of the melt, τ_{RM}, which can be calculated by [28-31]

$$\tau_{RM} = \frac{12 M \eta_{0M}}{\pi^2 \rho_M R(273°C + T_0)} \left(\frac{M_{cm}}{M} \right)^{2.4} \tag{14}$$

M_{cm} is the critical molar mass of PS in the melt state taken as 35,000 kg.mol^{-1} [32, 33]. The scaling relation for the Rouse time of the polymer solutions, τ_R, is then given as [24]

$$\tau_R(T_e) = \tau_{RM}(T_0) a_M^{2/3.4} a_T a_{Tg} \tag{15}$$

which by use of Eqs. 5-7 is equivalent to

$$\tau_R(T_e) = \frac{12 M_s \eta_0(T_e)}{\pi^2 \rho R(273°C + T_e)\varphi} \left(\frac{M_{cm}}{M_s \varphi} \right)^{2.4} \tag{16}$$

The values of τ_{RM} and $\tau_R$are also reported in Tables 1 and 2.

According to Baumgaertel, Schausberger and Winter (BSW) [34], only the terminal and glassy relaxation times as well as the plateau modulus are needed to determine the continuous relaxation spectrum $H(\tau)$ as the sum of entanglement contribution $H_e(\tau)$ and glassy contribution $H_g(\tau)$,

$$H(\tau) = H_e(\tau) + H_g(\tau) \tag{17}$$

with

$$H_e(\tau) = n_e G_N \left(\frac{\tau}{\tau_t}\right)^{n_e} h(1-\tau/\tau_t) \tag{18a}$$

and

$$H_g(\tau) = n_e G_N \left(\frac{\tau}{\tau_c}\right)^{-n_g} h(1-\tau/\tau_t) \tag{18b}$$

$h(x)$ is the Heaviside step function. The power law exponents n_e and n_g are associated with the entanglement region and the glass transition, respectively. Following Huang et al. [22, 23], the values of n_e and n_g are fixed to 0.23 and 0.70. The other characteristic material constants of the BSW model for the PS solutions are given by the scaling relations (11-13), and are summarized in Tables 1 and 2. Therefore, the BSW relaxation modulus is fully defined by

$$G(t) = G_e(t) + G_g(t) = \int_0^\infty \frac{H_e(\tau) + H_g(\tau)}{\tau} \exp(-t/\tau) d\tau = \int_0^\infty \frac{H(\tau)}{\tau} \exp(-t/\tau) d\tau \tag{19}$$

From the relaxation modulus, the storage (G') and loss (G") modulus can be obtained, and predictions are compared with experimental evidence [1] for the solutions PS3900/DEP-10 and PS3900/DEP-15 in Fig. 4. Agreement is found to be excellent for PS3900/DEP-10, and satisfactory for PS3900/DEP-15, considering that the predictions for the solutions with polymer concentrations of 0.1 and 0.15wt% at T_e=21.5°C were obtained by scaling from the reference melt PS-545k at T_0=130°C.

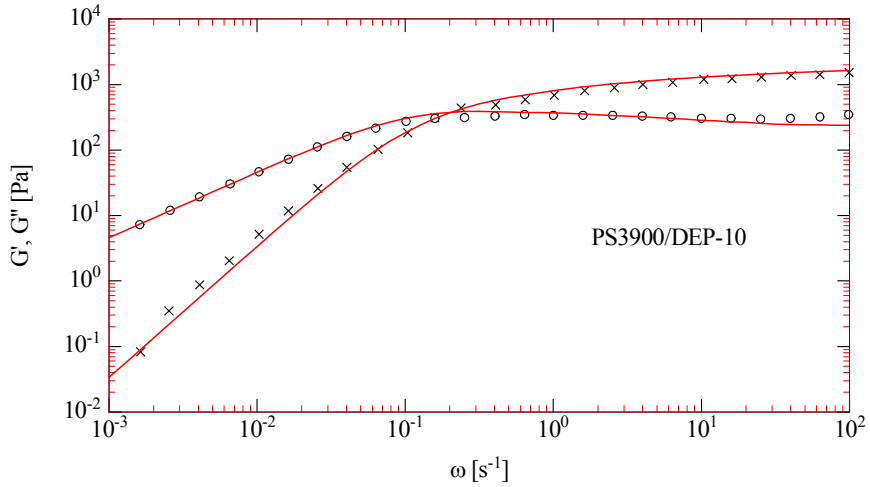

FIGURE 4a. Experimental data of storage (G', crosses) and loss (G", open circles) modulus for solution PS3900/DEP-10 at 21.5°C taken from Bhattacharjee et al. [1], and comparison (lines) to predictions by scaling from data of melt PS-545k at 130°C by use of the scaling Eq. 11-13.

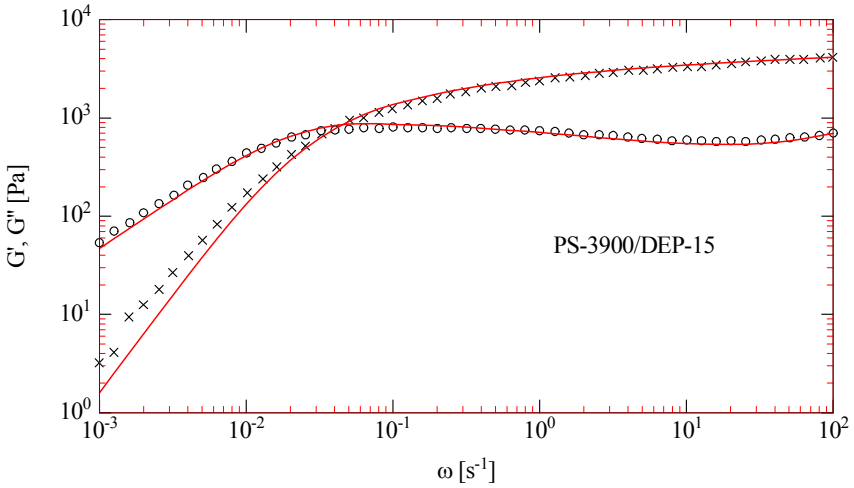

FIGURE 4b. Experimental data of storage (G', crosses) and loss (G", open circles) modulus for solution PS-3900/DEP-15 at 21.5°C taken from Bhattacharjee et al. [1], and comparison (lines) to predictions by scaling from data of melt PS-545k at 130°C by use of the scaling Eq. 11-13.

DOI-EDWARDS AND MSF MODEL

According to the tube model of Doi and Edwards (DE) [6], the diameter a_0 of the tube is constant, or equivalently the tension in the macromolecular chain remains constant and equal to its equilibrium value even for nonlinear deformations. The extra stress tensor $\boldsymbol{\sigma}(t)$ is then a consequence of the orientation of tube segments due to the flow. The resulting constitutive equation is of the single integral form,

$$\boldsymbol{\sigma}(t) = \int_{-\infty}^{t} \frac{\partial G(t-t')}{\partial t'} \mathbf{S}_{\mathrm{DE}}^{\mathrm{IA}}(t,t')\,dt' \tag{20}$$

if the tube segments are assumed to align independently of each other in the flow field (the "Independent Alignment (IA)" approximation). $G(t)$ is the linear-viscoelastic shear relaxation modulus with, and the relative strain measure $\mathbf{S}_{\mathrm{DE}}^{\mathrm{IA}}$ is given by

$$\mathbf{S}_{\mathrm{DE}}^{\mathrm{IA}}(t,t') \equiv 5\left\langle \frac{\mathbf{u}'\mathbf{u}'}{u'^2} \right\rangle_{\mathrm{o}} = 5\mathbf{S}(t,t') \tag{21}$$

$\boldsymbol{S}$ is the relative second order orientation tensor. The bracket denotes an average over an isotropic distribution of unit vectors $\mathbf{u}(t')$ at time t', and can be expressed as a surface integral over the unit sphere,

$$\langle\ \rangle_{\mathrm{o}} \equiv \frac{1}{4\pi} \oiint [\ ] \sin\theta_{\mathrm{o}}\, d\theta_{\mathrm{o}}\, d\phi_{\mathrm{o}} \tag{22}$$

At the observation time t, the unit vectors are deformed to vectors $\mathbf{u}'$, which are calculated from the affine deformation hypothesis (with $\mathbf{F}^{-1}(t,t')$ as the relative deformation gradient tensor) as

$$\mathbf{u}'(t,t') = \mathbf{F}^{-1}(t,t').\mathbf{u}(t') \tag{23}$$

u' indicates the length of the vector $\mathbf{u}'$.

The DE model does not account for any strain hardening. This is demonstrated in Fig. 5, where predictions of the DE model are compared to the steady-state elongational data of PS285k. As expected, prediction and data deviate increasingly with increasing strain rate, as the DE prediction scales with $\dot{\varepsilon}^{-1}$, while the data scale approximately with $\dot{\varepsilon}^{-1/2}$.

Doi and Edwards [6] added a stretch process with a stretch λ of the tube segments to their model in order to explain the discrepancies of the DE theory at start-up of shear and extensional flows. Pre-averaging the stretch, i.e. assuming that the stretch is uniform along the chain contour length and an explicit function $\lambda(t)$ of the observation time, the extra stress tensor is given by

$$\boldsymbol{\sigma}(t) = \lambda^2(t) \int_{-\infty}^{t} \frac{\partial G(t-t')}{\partial t'} \mathbf{S}_{\mathrm{DE}}^{\mathrm{IA}}(t,t')dt' \tag{24}$$

Eq. 24 required finding a stretch evolution equation, and a vast variety of concepts based on different kinetic ideas have been proposed in recent years [6, 7, 9, 35]. However, it should be noted that Eq. 24 with any function $\lambda^2(t)$ is not in agreement with experimental results of reversed elongational flow of a monodisperse polystyrene melt [36].

While in models with pre-averaged stretch, the tube diameter is always assumed to stay constant and equal to its equilibrium value a_o, stretch can also be introduced by the assumption of a strain-dependent tube diameter, as first suggested by Marrucci and de Cindio [37]. In this way, also the pre-averaging of the stretch can be avoided, which is inherently present in models based on Eq. 24 or its differential approximations. A generalized tube model with strain-dependent tube diameter was presented by Wagner and Schaeffer [38-40], and Wagner et al. [41]. In the Molecular Stress Function (MSF) theory, tube segment stretch $f = f(t,t')$ is the inverse of the relative tube diameter a,

$$f(t,t') = a_0 / a(t,t') \tag{25}$$

which decreases from its equilibrium value a_o with increasing stretch. Taking into account that the tube diameter a represents the mean field of the surrounding chains, it is assumed that the tube diameter is independent of the orientation of tube segments. The extra stress is then given as

$$\boldsymbol{\sigma}(t) = \int_{-\infty}^{t} \frac{\partial G(t-t')}{\partial t'} f^2 \mathbf{S}_{DE}^{IA}(t,t')dt' \tag{26}$$

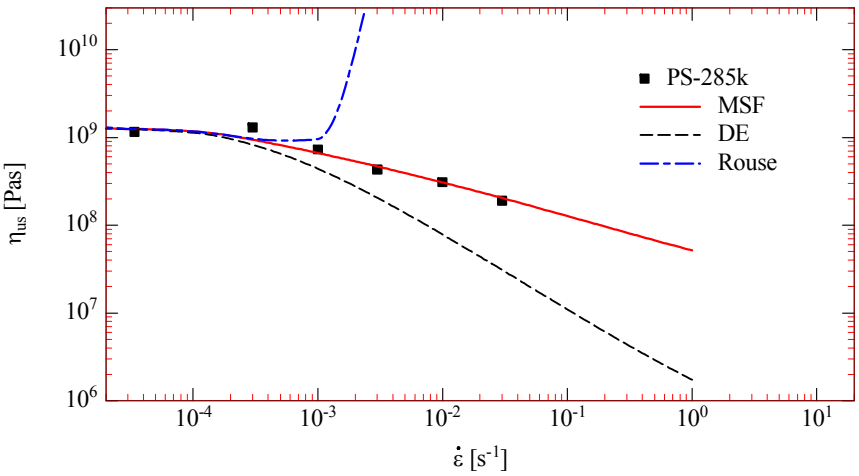

FIGURE 5. Comparison of steady-state elongational viscosity data of PS-285k (full symbols) to predictions by DE theory (dashed line), Eq. 20, Rouse stretch (dash-dotted line) according to evolution Eq. 27, and MSF model (full line) according to evolution Eq. 37.

In contrast to Eq. 24, stretch in Eq. 26 does not only depend on the observation time t, but depends on the strain history, i.e. for time-dependent strain histories, chain segments with long relaxation times (i.e. at the center of the chain) see higher stretches than chain segments with short relaxation times (i.e. at the chain ends).

If we follow conventional arguments [7] and assume that the (on average) affine deformation of the chain is balanced by a linear entropic spring force, the evolution equation for f takes the form

$$\frac{\partial f}{\partial t} = f(\kappa : \mathbf{S}) - \frac{1}{\tau_{\mathrm{Rm}}}(f-1) \tag{27}$$

with the initial condition $f(t = t', t') = 1$. κ is the velocity gradient and **S** the orientation tensor. However, this evolution equation does not describe the steady-state elongational viscosity of monodisperse PS melts with Rouse stretch relaxation times τ_{RM} [21]. As demonstrated in Fig. 5 for PS-285k, a linear spring force will quench chain stretch as long as the Weissenberg number $Wi_{Rm} = \dot{\varepsilon}\,\tau_{Rm}$ is smaller than 1, while chain stretch will diverge in the limit of $Wi_{\mathrm{Rm}} \rightarrow 1$, resulting in a diverging steady-state elongational viscosity. This is clearly seen by setting the left hand side of Eq. 27 to zero, which gives the maximum stretch $f_{\max}$ as

$$f_{\max} = \frac{1}{1 - \dot{\varepsilon}\tau_{Rm}} \tag{28}$$

We will not discuss finite extensibility here, which is usually invoked to rectify the situation to some degree and to remove the singularity. According to the analysis of Rolón-Garrido et al. [18], finite extensibility has only a minor effect on the transient elongational stress, while it has a significant effect on birefringence and the stress optical rule.

THE INTERCHAIN TUBE PRESSURE

Doi and Edwards [6] showed that the pressure exerted by the chain on the walls of a box is anisotropic, if the chain is confined to an anisotropic box. For a tube with circular cross section, this leads to a relative radial pressure p/p_0 which increases inversely proportional to the 3rd power of the tube diameter a from its equilibrium value p_0 [14, 15],

$$\frac{p}{p_0} = \frac{a_0^3}{a^3} \tag{29}$$

Therefore, when the tube diameter is decreased with increasing deformation, the radial pressure of the chain exerted on the surrounding topological constraints, the so-called "interchain pressure", is increasing and is balancing the tube diameter reduction caused by elongational flow with strain rate $\dot{\varepsilon}$ [14],

$$\frac{\partial a}{\partial t} = -\dot{\varepsilon}\,a + \frac{a_0}{\tau_{\mathrm{a}}}\left(\frac{a_0^3}{a^3} - 1\right) \tag{30}$$

We called τ_{a} the tube diameter relaxation time, and replaced the first term on the right hand side by the general tensorial description for the deformation rate [16]. Inserting the definition of the molecular stress function, $f = \frac{a_0}{a}$, we obtained the following evolution equation for the tension in a chain segment,

$$\frac{\partial f}{\partial t} = f(\kappa : \mathbf{S}) - \frac{f^2\left(f^3 - 1\right)}{\tau_a} \tag{31}$$

with the initial condition $f(t = t', t') = 1$. When the linear-viscoelastic response is known, Eq. 31 together with Eq. 26 represent a full constitutive relation with only one material parameter, the tube diameter relaxation time τ_{a}.

Due the nonlinear restoring pressure term on the right hand side of Eq. 31, the divergence of the maximum stretch $f_{\max}$ in constant strain-rate elongation is now removed, and for fast deformations, the steady-state elongational viscosity scales with

$$\eta_{\mathrm{us}} \propto \sqrt{\tau_a}\,\dot{\varepsilon}^{-\frac{1}{2}} \tag{32}$$

in correspondence to the experimental results of Bach et al. [4].

THE EXTENDED INTERCHAIN TUBE PRESSURE MODEL

The interchain tube pressure approach of Marrucci and Ianniruberto [14] considers only the force balance in the lateral direction of the tube. The original findings of Doi and Edwards [6], however, maintain that the chain pressures on the walls of a confining box are anisotropic if the dimensions of the box are anisotropic, i.e. we expect different restoring effects in the longitudinal direction (tube axis) due to Rouse relaxation of the chain, and in the lateral direction of the tube due to the interchain pressure. Therefore, we made the constitutive assumption that chain stretch is balanced simultaneously and additively by three restoring effects, one in the z-direction (tube axis), R_z, and two in the lateral x- and y-directions, R_x and R_y (see Fig. 6), with

$$R_x = R_y = \frac{f^2\left(f^3-1\right)}{\tau_a} \tag{33}$$

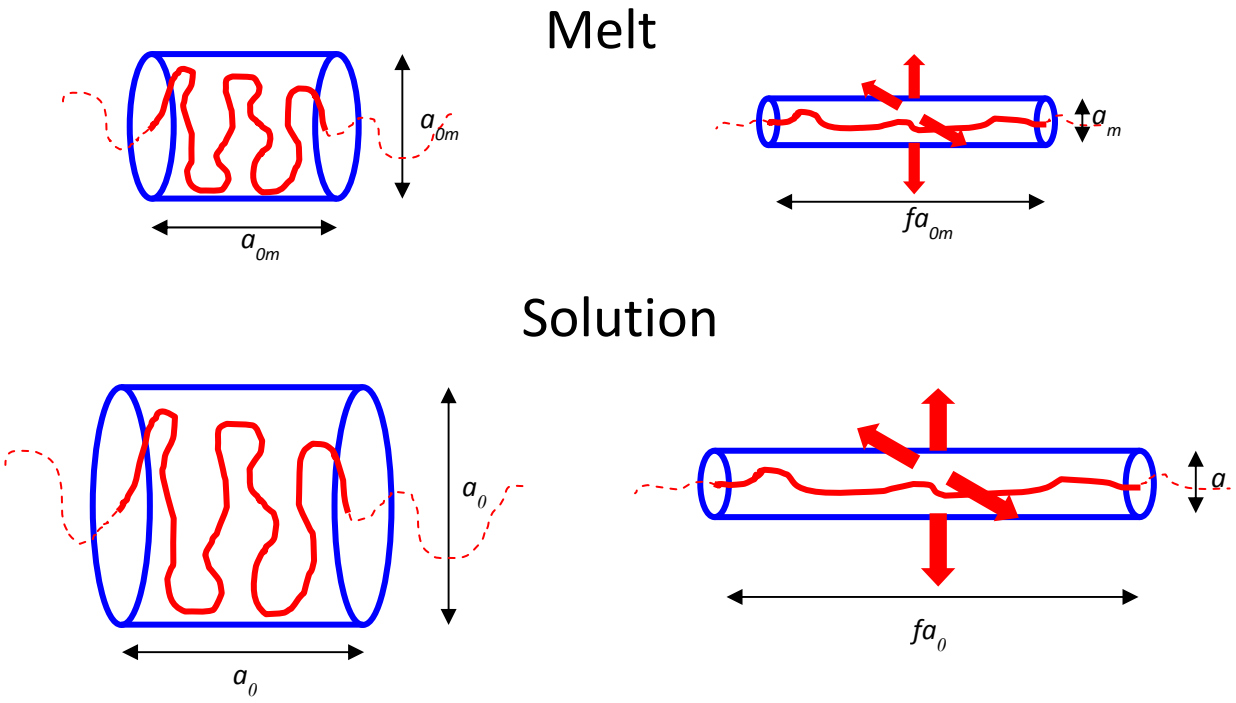

FIGURE 6. Similarity of tube segment deformation for melt and solution. For details see text.

In the melt, R_x, R_y and R_z carry a weight fraction of 1/3 each [19, 20]. In solution, we assume that the interchain pressure effects in the x- and y-direction still have a weight fraction of 1/3 each, while the weight of the longitudinal Rouse relaxation is determined from the condition that in the limit of small stretch, i.e. $f\text{-}1<<1$, the classical relation

$$\frac{\partial f}{\partial t} = f\left(\kappa : \mathbf{S}\right) - \frac{1}{\tau_R}(f-1) \tag{34}$$

is retained. This leads to the evolution equation for the molecular stress function f of the extended interchain pressure (EIP) model,

$$\frac{\partial f}{\partial t} = f\left(\kappa : S\right) - R_z - \frac{2}{3}R_x = f\left(\kappa : \mathbf{S}\right) - \left(1-2\frac{\tau_R}{\tau_a}\right)\frac{f-1}{\tau_R} - \frac{2}{3}\frac{f^2\left(f^3-1\right)}{\tau_a} \tag{35}$$

Considering that $f^2(f^3-1)$ reduces to $3(f-1)$ for $f-1 \ll 1$, Eq. 35 is equivalent to Eq. 34 for small stretch.

In the case of the melt and in agreement with experimental evidence, Wagner and Rolón-Garrido [19, 20] reported an evolution equation of the form

$$\frac{\partial f}{\partial t} = f(\kappa : \mathbf{S}) - \frac{1}{3}\frac{f-1}{\tau_{\mathrm{Rm}}} - \frac{2}{3}\frac{f^2\left(f^3-1\right)}{3\tau_{\mathrm{Rm}}} \tag{36}$$

i.e. the tube diameter relaxation time τ_{a} is equal to three times the Rouse time τ_{Rm} of the melt, $\tau_{\mathrm{a}}=3\tau_{\mathrm{Rm}}$. Eq. 36 is equivalent to the classical relation (Eq. 34) in first order in the stretch. It removes the singularity present in the classical relation for $Wi_{\mathrm{Rm}} \to 1$. It does not contain any nonlinear material parameter, as the Rouse time τ_{Rm} of the chain is determined by the molecular characteristics of the polymer melt as obtained from linear viscoelasticity. As the interchain pressure term enters in Eq. 36 with the weight of 2/3, the effective tube diameter relaxation time of the melt is $\frac{9}{2}\tau_{\mathrm{Rm}}$, and this was found to be in excellent agreement with elongational viscosity data of the melts PS390K and PS200K [19, 20], and it also in agreement with melt PS-285k (Figs. 5 and 8) and PS-545k (Fig. 9). In elongational flow, Eq. 36 is equivalent to

$$\frac{\partial f}{\partial \varepsilon} = f(S_{11} - S_{33}) - \frac{1}{3}\frac{f-1}{Wi_{\mathrm{RM}}} - \frac{2}{3}\frac{f^2\left(f^3-1\right)}{3Wi_{\mathrm{RM}}} \tag{37}$$

ε is the Hencky strain, S_{11} and S_{33} are tensor components of the orientation tensor, and $Wi_{\mathrm{RM}} = \dot{\varepsilon}\,\tau_{\mathrm{RM}}$ is the Weissenberg number based on the Rouse time of melt. Obviously, for thermo-rheological simple fluids such as linear polystyrene, Eq. 37 is temperature invariant. We note that for $Wi_{\mathrm{RM}} = \dot{\varepsilon}\,\tau_{\mathrm{RM}} \gg 1$, the (temperature-invariant) elongational stress σ is given by

$$\sigma \cong 5G_{\mathrm{NM}} f^2 = \frac{15}{2} G_{\mathrm{NM}} \sqrt{2Wi_{\mathrm{RM}}} \tag{38}$$

We now consider the evolution equation in the case of solutions. For a dilution exponent of $\alpha = 1$ [22, 23], the following relations hold:

$$a_0 = a_{0\mathrm{m}}\,\phi^{-1/2} \tag{39}$$

$$a = a_{\mathrm{m}}\,\phi^{-1/2} \tag{40}$$

From Eq. 30, the relative interchain tube pressure in solution is then the same as in the melt state,

$$\frac{p}{p_0} = \frac{a_0^3}{a^3} = \frac{a_{0\mathrm{m}}^3}{a_{\mathrm{m}}^3} \tag{41}$$

provided that in solution the polymer chains are still entangled. As far as the lateral direction is concerned, for any polymer volume fraction φ the change of the topological restrictions due to deformation is self-similar to the condition of the melt state (see Fig. 6). Therefore we expect that the evolution equation of the stretch is the same for melts and solutions. Due to the shift in the glass transition temperature, the Rouse time of the solutions is much smaller than the Rouse time of the melts. We assume that the additional free volume created by the solvent speeds up Rouse relaxation along the tube axis, but does not affect the interchain tube pressure created by binary contacts of polymer chains. The tube diameter relaxation of the solutions is then the same as in the melt state, resulting from Eq. 35 in an evolution equation of the form

$$\frac{\partial f}{\partial t} = f(\kappa : \mathbf{S}) - (1 - \frac{2}{3}\frac{\tau_{\mathrm{R}}}{\tau_{\mathrm{Rm}}})\frac{f-1}{\tau_{\mathrm{R}}} - \frac{2}{3}\frac{f^2\left(f^3-1\right)}{3\tau_{\mathrm{Rm}}} \tag{42}$$

This means that even in the case of solutions, the interchain tube pressure is characterized by the Rouse time of the corresponding melt at the reference temperature T_0=130°C. By use of Eq. 15, τ_{Rm} can also be expressed in terms of the Rouse time τ_R of the solution as $\tau_{Rm} = \tau_R a_{Tg}^{-1}$, leading to an alternative formulation of the evolution equation in terms of the Rouse time τ_R of the solution,

$$\frac{\partial f}{\partial t} = f(\kappa:\mathbf{S}) - \left(1 - \frac{2}{3}a_{Tg}\right)\frac{f-1}{\tau_R} - \frac{2}{3}a_{Tg}\frac{f^2\left(f^3-1\right)}{3\tau_R} \tag{43}$$

Thus for concentrated solutions, where due to a reduction of the glass transition temperature the Rouse time of the solution is reduced by a factor a_{Tg} relative to the Rouse time of the melt, the interchain tube pressure effect expressed in terms of τ_R is reduced by the same factor, and the Rouse relaxation in the longitudinal direction is enhanced. Eqs. 42 and 43 contain Eq. 36 in the limit of the melt state, i.e. for $\tau_R = \tau_{Rm}$, corresponding to a_{Tg}=1. For high Weissenberg number elongational flows with $Wi_R = \dot{\varepsilon}\,\tau_R >> 1$, the elongational stress for PS/OS solutions is then given by

$$\sigma \cong 5G_N f^2 = \frac{15}{2}G_N\sqrt{2\frac{Wi_R}{a_{Tg}}} = \frac{15}{2}G_{NM}\phi^2\sqrt{2Wi_{RM}} \tag{44}$$

The (temperature-invariant) elongational stress of the solutions is limited by the interchain pressure of the PS macromolecules in the same way as in the melt, except that the plateau modulus G_N of the solutions is reduced by dilution relative to the modulus G_{NM} of the melt. The validity of the limiting elongational stress for melts and solutions of PS-285k and PS-545k as investigated by Huang et al. [22, 23] is demonstrated in Fig. 7. The reduced elongational stress $\frac{\sigma\sqrt{a_{Tg}}}{G_{NM}\phi^2}$ calculated from the experimental steady-state elongational viscosity data, is plotted as a function of $Wi_R = \dot{\varepsilon}\,\tau_R$. Indeed, melts and solutions attain the same limiting reduced stress of $\frac{15}{2}\sqrt{2Wi_R}$ at higher Weissenberg numbers. Figs. 8 and 9 demonstrate the agreement between experimental data of the steady-state elongational viscosities of PS-285k und PS-545k and their solutions in oligomeric styrene and predictions of evolution Eq. 43.

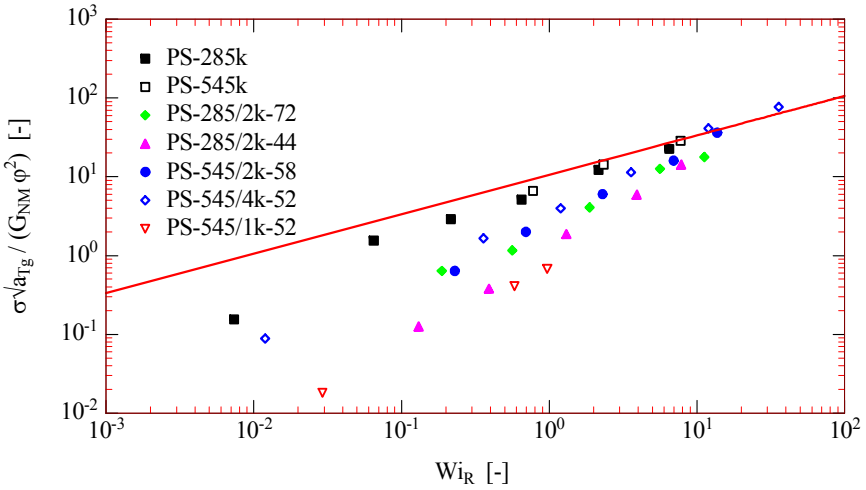

FIGURE 7. Reduced elongational stress as a function of $Wi_R = \dot{\varepsilon}\,\tau_R$ for polymer melts and solutions investigated by Huang et al. [22, 23]. Solid line is given by $\frac{\sigma\sqrt{a_{Tg}}}{G_{NM}\phi^2} = \frac{15}{2}\sqrt{2Wi_R}$.

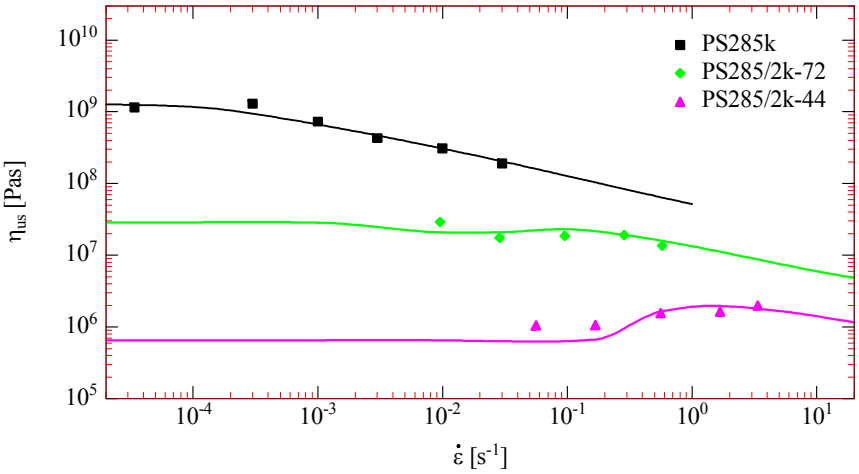

FIGURE 8. Steady-state elongational viscosity $\eta_{us}(\dot{\varepsilon})$ of PS-245k and solutions in 2k OS. Data (symbols) from Huang et al. [22]. Predictions (lines) by Eqs. 26 and 43.

COMPARISON TO ELONGATIONAL VISCOSITY DATA OF THE SYSTEMS PS-1950/DEP AND PS-3900/DEP

We will now use the constitutive relations (Eqs. 26 and 43) together with the relaxation modulus of Eq. 20 to model the steady-state elongational viscosity data of Bhattacharjee et al. [1] and Acharya et al. [12]. The data are presented in Figs. 10 and 11. A plateau of the elongational viscosity data is observed at small elongational rates for PS-1950/DEP and PS-3900/DEP-17, indicating three times the zero-shear viscosity. Subsequently, all the solutions show a decrease of the elongational viscosity followed by a drastic upturn.

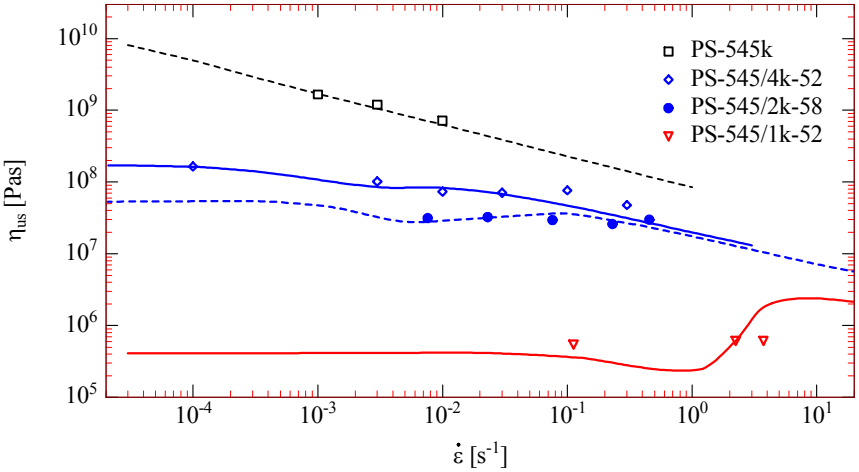

FIGURE 9. Steady-state elongational viscosity of PS-545k and solutions in 4k, 2k, and 1k OS at 130°C. Data (symbols) from Huang et al. [23]. Predictions (lines) by Eqs. 26 and 43.

In Fig. 10, predictions of Eqs. 26 and 43 are compared to the experimental elongational viscosity data of solutions PS-1950/DEP applying the Rouse relaxation time calculated from Eq. 16. While the data of PS-1950/DEP-10 are predicted quantitatively, the model describes only qualitatively the data for PS-1950/DEP-15 and PS-1950/DEP-20, i.e. a decrease of the elongational viscosity followed by a steep increase. According to the scaling relation (Eq. 16), the Rouse time τ_R increases with increasing polymer concentration, while the experimental data of

PS-1950/DEP seem to indicate that the upturn of the elongational viscosity takes place at a nearly constant value of the elongation rate. This may signify that for a good solvent such as DEP, relation (Eq. 16) is only approximately valid at higher polymer concentrations. We may add that also the Rouse times calculated by standard methods and reported by Acharya et al. [12], are larger than those observed experimentally except for PS-1950/DEP-10. An excellent description of the elongational viscosity data for PS-1950/DEP and PS-3900/DEP can be obtained when the Rouse relaxation time is fitted to the upturn of the elongational viscosity as shown in Fig. 11. The optimal values τ_{Rexp} as reported in Tables 1 and 2 are smaller than the values of τ_R calculated from Eq. 16 by a factor of 1/2 to 1/3, except for PS-1950/DEP-10.

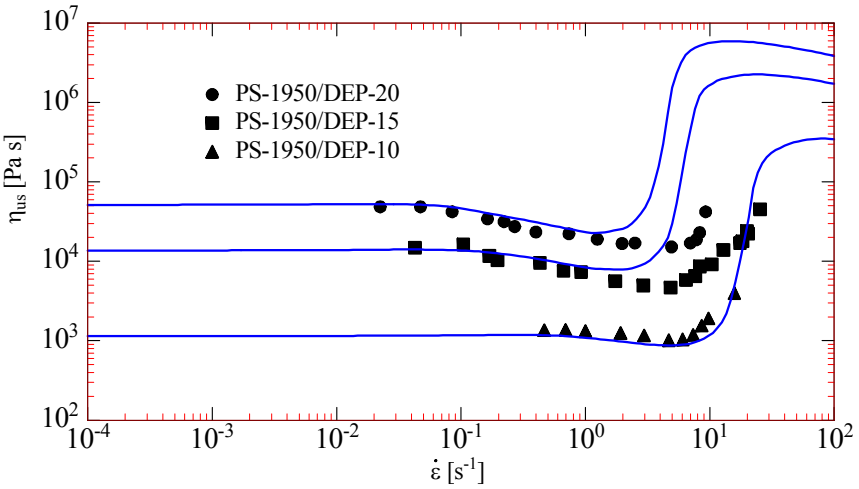

FIGURE 10. Steady-state elongational viscosity data (symbols) of solutions PS-1950/DEP compared to predictions (lines) of the EIP model with τ_R as calculated from Eq. 16.

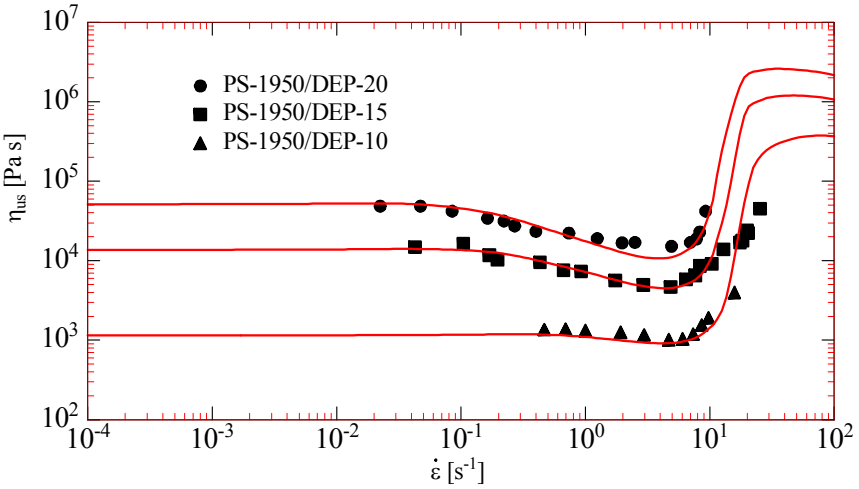

FIGURE 11a. Steady-state elongational viscosity data (symbols) of solutions PS-1950/DEP compared to predictions (lines) of the EIP model with the optimal Rouse times τ_{Rexp} reported in Tables 1 and 2.

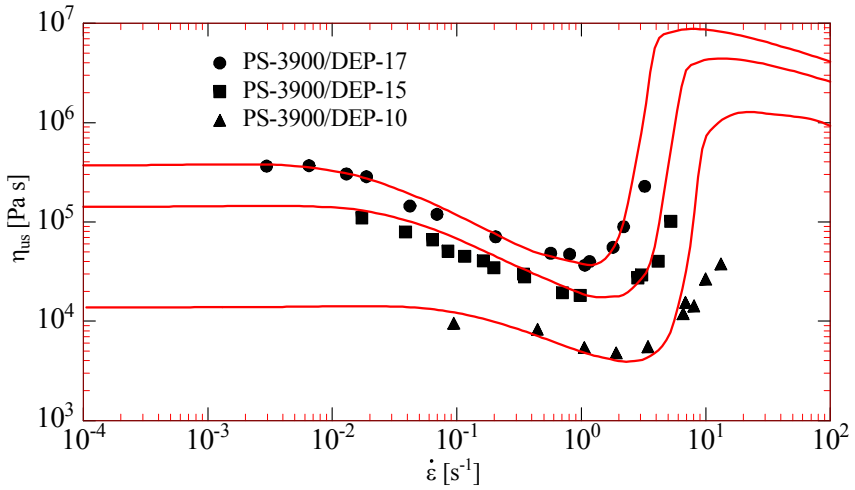

FIGURE 11b. Steady-state elongational viscosity data (symbols) of solutions 3900/DEP compared to predictions (lines) of the EIP model with the optimal Rouse times τ_{Rexp} reported in Tables 1 and 2.

According to the EIP model, the behaviour of the elongational viscosity of the PS/DEP solutions is governed by three timescales: (i) the reptation time represented by the terminal relaxation time τ_t; (ii) the Rouse time of the solution τ_R; and (iii) the tube diameter relaxation time expressed as $3\tau_R/a_{Tg}$, i.e. the Rouse time of the solution modified by the shift factor a_{Tg}, which represents the shift of the glass transition temperature from melt to solution. The drop of the viscosity corresponds to tube segment orientation for $Wi_t = \dot{\varepsilon}\,\tau_t \geq 1$ with no or little stretch, i.e. in the regime $Wi_R = \dot{\varepsilon}\,\tau_R < 1$, while the steep upturn follows at $Wi_R = \dot{\varepsilon}\,\tau_R \to 1$. Therefore, the decrease in the elongational viscosity is more pronounced, when the difference between τ_t and τ_R is larger. For PS-1950/DEP-10, no significant initial dip in the elongational viscosity is seen. This is due to the fact that for this solution, the difference between τ_t and τ_R with a ratio of $\tau_t/\tau_R \equiv 16$ is too small, and therefore tube segment orientation and stretch are not well separated. The maximum and the transition to the final scaling of $(\dot{\varepsilon}\tau_R / a_{Tg})^{-1/2}$ in the prediction is caused by the interchain tube pressure at $Wi_R = \dot{\varepsilon}\,\tau_R >> 1$, which is outside the range of the available experimental data.

CONCLUSIONS

The scaling relations established for the relaxation modulus of concentrated solutions of polystyrene in oligomeric styrene with polymer volume fractions of 44 to 72% [24, 25] are applicable to the system of PS/DEP investigated by Bhattacharjee et al. [1] and Acharya et al. [12] at polymer concentrations of 10 to 20%. The scaling relies on the difference $\Delta T_g = T_{gm} - T_{gs}$ of the glass-transition temperature T_{gm} of the melt and the glass-transition temperatures T_{gs} of the solutions. ΔT_g can be inferred from the reported zero-shear viscosities, and the BSW spectra of the solutions are obtained from the BSW spectrum of the reference melt with good accuracy. This means that to predict linear viscoelasticity of a solution with polymer concentration φ, only the linear-viscoelastic characteristics of a reference polystyrene melt and the shift ΔT_g of the glass transition temperature are needed.

By use of the Extended Interchain Pressure (EIP) model [24, 25], which is based on the fact that the relative interchain pressure in the melt and in the solutions is identical, the steady-state elongational viscosity data of PS-3900 and PS-1950 dissolved in DEP at concentrations between 10 and 20% can be modeled qualitatively, and for PS-1950/DEP-10 even quantitatively. For the other solutions considered, the Rouse stretch relaxation times as calculated from the respective scaling relation are a factor of 2 to 3 higher than the Rose times defined by the experimentally observed upturn of the elongational viscosities at $Wi_R = \dot{\varepsilon}\,\tau_R \to 1$. This may be caused by DEP being a good solvent for polystyrene at room temperature. Using the experimentally determined Rouse times, quantitative agreement between experimental data and model is obtained.

Except for the possible influence of solvent quality, linear and nonlinear viscoelasticity of an entangled polystyrene solution can thus be obtained from the linear-viscoelastic characteristics of a reference polymer melt and the shift of the glass transition temperature between melt and solution. As an example, Fig. 12 shows the

elongational viscosity of a hypothetical polystyrene PS-1500k with molar mass of 1500 kmol.g^{-1} dissolved in 1k oligomeric styrene at 130°C with polymer fractions from 1 down to 0.2. By dissolution in oligomeric styrene, a possible impact of solvent quality is avoided. The shift ΔT_g in the glass transition temperature is given by Eq. 3, and the shift factor a_{Tg} by Eq. 2.

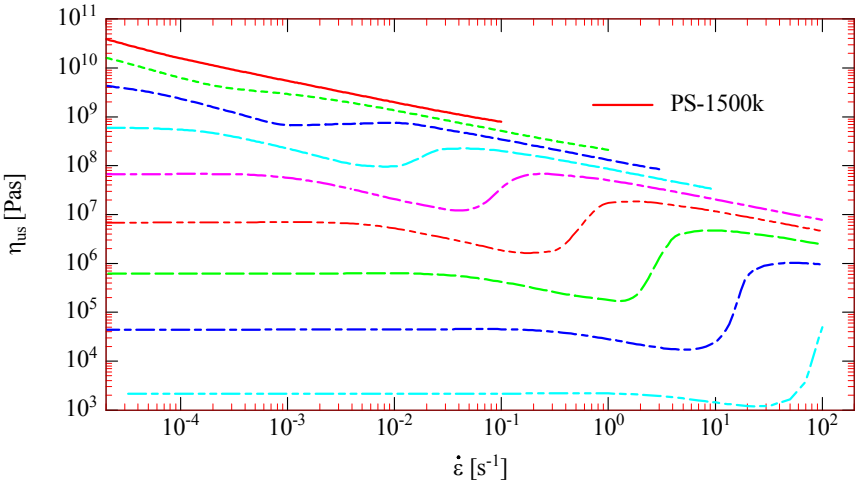

FIGURE 12. Elongational viscosity of hypothetical melt PS-1500k dissolved in 1k oligomeric styrene at 130°C. Polymer fractions from top to bottom: 1, 0.9, 0.8, 0.7, 0.6, 0.5, 0.4, 0.3, 0.2.

While the melt PS-1500k and the solution PS-1500/1k-90 show a continuously deceasing trend with a scaling of $(\dot{\varepsilon}\tau_R / a_{Tg})^{-1/2} = (Wi_{RM})^{-1/2}$ at higher elongation rates, the solutions from PS-1500/1k-80 to PS-1500/1k-50 feature a decrease followed by an upturn, which is the more pronounced the lower the polymer concentration. The elongational viscosity of PS-1500/1k-80 and PS-1500/1k-70 are in principal agreement with the experimental results of Huang et al. [22, 23], while PS-1500/1k-30 and PS-1500/1k-20 feature the behaviour of the PS-1950/DEP and PS-3900/DEP solutions investigated by Bhattacharjee et al. [1]. At lower polymer concentrations, the difference between τ_t and τ_R becomes smaller, and the dip in the elongational viscosity is reduced, while the upturn continues to increase in line with the decreasing significance of the interchain pressure relative to Rouse relaxation. Thus, the scaling relations presented together with the constitutive relations of the EIP model allow for a consistent prediction of the transition from melt to concentrated solution based exclusively on the linear-viscoelastic characteristics of a reference melt and the shift of the glass transition temperature from melt to solution.

We conclude with the statement that the experimental data in elongational flow of monodisperse polystyrene melts and their solutions in different solvents are consistent with the assumption that the tube, i.e. the confinement of a test chain, is characterized by the orientation in the direction along the tube, and the diameter of the tube in the lateral dimension. Chain stretch is associated with a reduction of the tube diameter, and is balanced by a linear spring force in the longitudinal direction and a nonlinear interchain tube pressure in the lateral direction. This leads to two basic constitutive relations, namely the expression for the stress tensor, Eq. 26,

$$\boldsymbol{\sigma}(t) = \int_{-\infty}^{t} \frac{\partial G(t-t')}{\partial t'} f^2 \mathbf{S}_{DE}^{IA}(t,t')dt'$$

and the evolution equation for stretch of melts ($a_{Tg} = 1$, $\tau_t = \tau_R$) and solutions ($a_{Tg} < 1$), Eq. 43,

$$\frac{\partial f}{\partial t} = f(\kappa:\mathbf{S}) - \left(1 - \frac{2}{3}a_{Tg}\right)\frac{f-1}{\tau_R} - \frac{2}{3}a_{Tg}\frac{f^2\left(f^3-1\right)}{3\tau_R}$$

These equations are of exceptional simplicity and beauty. The extra stress is given by a history integral of the stress created by tube segments as characterized by linear viscoelasticity through $G(t)$, which are stretched and oriented. It is important to note the stretch is inside the integral, i.e. it is a relative quantity. Chain stretch f is

associated with a reduction of the tube diameter, and is balanced by a linear spring force in the longitudinal direction and a nonlinear interchain tube pressure in the lateral direction. Dilution of the polymer by a solvent does not reduce the relative interchain tube pressure. Once $G(t)$ of a linear, monodisperse, well-entangled polymer melt and its solution are known, the Rouse stretch relaxation time of the melt, τ_{Rm}, and of the solution, τ_R, are given by Eq. 6, and there are no free parameters.

By dilution of the polymer with a solvent, the glass transition temperature T_g of the polymer in solution is reduced relative to T_g of the melt. By use of appropriate scaling relations, quantitative agreement between highly nonlinear viscoelastic experiments and predictions for polystyrene melts and concentrated solutions of polystyrene can be obtained based exclusively on the relaxation modulus $G_m(t)$ of the polymer melt, the volume fraction φ of polymer in the solution and the time-temperature shift factor a_{Tg} quantifying the reduction of the glass transition temperature T_g of the polymer in solution relative to T_g of the melt.

ACKNOWLEDGMENTS

Financial support by the German Science Foundation is gratefully acknowledged.

REFERENCES

1. P. K. Bhattacharjee, J. P. Oberhauser, G. H. McKinley, L. G. Leal and T. Sridhar, Macromolecules **35**, 10131-10148 (2002).
2. P. K. Bhattacharjee, D. A. Nguyen, G. H. McKinley and T. Sridhar, J. Rheol. **47**, 269-290 (2003).
3. G. McKinley and T. Sridhar, Ann. Rev. Fluid Mech. **34**, 375-415 (2002).
4. A. Bach, K. Almdal, H. K. Rasmussen and O. Hassager, Macromolecules **36**, 5174-5179 (2003).
5. J. K. Nielsen, H. K. Rasmussen and O. Hassager, J. Rheol. **52**, 885-899 (2008).
6. M. Doi and S. F. Edwards, *The Theory of Polymer Dynamics* (Oxford University Press, Oxford, 1986).
7. D. S. Pearson, A. Kiss, L. Fetters and M. Doi, J. Rheol. **33**, 517-535 (1989).
8. D. W. Mead, D. Yavich and L. G. Leal, Rheol. Acta **34**, 360-383 (1995).
9. D. W. Mead, R. G. Larson and M. Doi, Macromolecules **31**, 7895-7914 (1998).
10. J. Fang, M. Kröger and H. C. Öttinger, J. Rheol. **44**,1293-1317 (2000).
11. P. S. Desai and R. G. Larson, J. Rheol. **58**, 255-279 (2014).
12. M. V. Acharya, P. K. Bhattacharjee, D. A. Nguyen, T. Sridhar, "Are entangled polymeric solutions different from melts?", in The XV International Congress on Rheology. AIP Conference Proceedings **1027**, edited by A. Co et al. (American Institute of Physics, Melville, NY, 2008), pp. 391-393.
13. T. Sridhar, M. Acharya, D. A. Nguyen and P. K. Bhattacharjee, Macromolecules **47**, 379-386 (2014).
14. G. Marrucci and G. Ianniruberto, Macromolecules **37**, 3934-3942 (2004).
15. G. Marrucci and G. Ianniruberto, Korea-Australia Rheol. J. **17**, 111-116 (2005).
16. M. H. Wagner, S. Kheirandish and O. Hassager, J. Rheol. **49**, 1317-1327 (2005).
17. O. Hassager, "Polymer fluid mechanics: Molecular orientation and stretching," in *The XIVth International Congress on Rheology*, Conference Proceedings, (The Korean Society of Rheology, Seoul, Korea, 2004), pp. 58.
18. V. H. Rolón-Garrido, M. H. Wagner, C. Luap and T. Schweizer, J. Rheol. **50**, 327-340 (2006).
19. M. H. Wagner and V. H. Rolón-Garrido, "Recent advances in constitutive modeling of polymer melts," in *Novel Trends in Rheology III*, AIP Conference Proceedings 1152, ed. by M. Zatloukal (American Institute of Physics, Zlin, 2009), pp.16-31.
20. M. H. Wagner and V. H. Rolón-Garrido, Korea-Australia Rheol. J. **21,** 203-211 (2009).
21. M. H. Wagner, J. Non-Newtonian Fluid Mech. **166**, 915-194 (2011).
22. Q. Huang, O. Mednova, H. K. Rasmussen, N. J. Alvarez, A. L. Skov, K. Almdal and O. Hassager, Macromolecules **46**, 5026-5035 (2013).
23. Q. Huang, N. J. Alvarez, Y. Matsumiya, H. K. Rasmussen, H. Watanabe and O. Hassager, ACS Macro Letters **2**, 741-744 (2013).
24. M. H. Wagner, Rheol. Acta **53**, 765-777 (2014).
25. M. H. Wagner, J. Non-Newtonian Fluid Mech. http://dx.doi.org/10.1016/j.jnnfm.2014.09.017 (2014).
26. D. A. Savin, A. M. Larson and T. P. Lodge, J. Polym. Phys. B **42**, 1155-1163 (2004).
27. T. G. Fox and P. J. Flory, J. Appl. Phys. **21**, 581-591 (1950).

28. K. Osaki, K. Nishizawa and M. Kurata, Macromolecules **15**, 1068-1071 (1982).
29. E. V. Menezes and W. W. Graessley, J. Polym. Sci.: Polym. Phys. **20**, 1817-1833 (1982).
30. M. Takahashi, T. Isaki, T. Takigawa and T. Masuda, J. Rheol. **37**, 827-846 (1993).
31. T. Isaki, M. Takahashi and O. Urakawa, J. Rheol. **47**, 1201-1210 (2003).
32. J. D. Ferry, *Viscoelastic Properties of Polymers* (Wiley, New York, 1980).
33. C. Luap, C. Müller, T. Schweizer and D. C. Venerus, Rheol. Acta **45**, 83−91 (2005).
34. M. Baumgaertel, A. Schausberger and H. H. Winter, Rheol. Acta **29**, 400-408 (1990).
35. T. C. B. McLeish and R. G. Larson, J. Rheol. **42**, 81-110 (1998).
36. J. K. Nielsen and H. K. Rasmussen, J. Non-Newtonian Fluid Mech. **155**, 15-19 (2008).
37. G. Marrucci and B. de Cindio, Rheol. Acta **19**, 68-75 (1980).
38. M. H. Wagner and J. Schaeffer, J. Rheol. **36**, 1-26 (1992).
39. M. H. Wagner and J. Schaeffer, J. Rheol. **37**, 643-661 (1993).
40. M. H. Wagner and J. Schaeffer, Rheol. Acta. **33**, 506-516 (1994).
41. M. H. Wagner, P. Rubio and H. Bastian, J. Rheol. **45**, 1387-1412 (2001).